Final Draft
of the original manuscript:

Wang, H.; Colegrove, P.A.; dos Santos, J.F.:
Hybrid modelling of 7449-T7 aluminium alloy friction stir welded joints
In: Science and Technology of Welding and Joining (2013) Maney

DOI: 10.1179/1362171812Y.0000000078

Hybrid modelling of 7449-T7 aluminium alloy friction stir welded joints

H. Wang[1], Paul A. Colegrove[1], and Jorge dos Santos[2]

[1]Cranfield University, Cranfield, Bedfordshire MK43 0AL, United Kingdom
[2]Helmholtz-Zentrums Geesthacht, Institute of Materials Research, Materials Mechanics, Solid-State Joining Processes, Max-Planck-Str. 1, 21502 Geesthacht, Germany

Corresponding Author:

Hua Wang, present address: [2]Helmholtz-Zentrums Geesthacht, Institute of Materials Research, Materials Mechanics, Solid-State Joining Processes, Max-Planck-Str. 1, 21502 Geesthacht, Germany Phone: +494152872055. Fax: +494152872033. Email: hua.wang@hzg.de

Abstract

Many finite element models use adjustable parameters that control the heat loss to the backing bar as well as the heat input to the weld. In this paper we describe a method for determining these parameters with a hybrid artificial neural network (ANN) coupled thermal-flow process model of the friction stir welding (FSW) process. The method successfully determined temperature-dependent boundary condition parameters for a series of friction stir welds in 3.2-mm thick 7449 aluminium alloy. The success of the technique depended on: 1) the method used to input thermal data into the ANN and 2) the ANN topology. Using this technique to obtain the adjustable parameters of a model is more efficient than the conventional trial and error approach, especially where complex boundary conditions are implemented.

Keywords: modelling of friction stir welding, artificial neural networks, contact gap conductance, computational fluid dynamics, plunge depth

1 Introduction

In FSW modelling, two major approaches have been used to describe the heat loss from the workpiece to the backing bar. The first method simplifies the heat loss using a convective transfer and has been used by Khandkar et al.[1], Nandan et al.[2] and Arora et al.[3]. The second method uses a contact gap conductance to represent the imperfect contact at the interface between the workpiece and the backing bar[1, 4, 5]. The contact gap conductance, k is defined as: $k = Q/(T_0-T_A)$, where Q is the heat flux from the workpiece to the backing bar, T_O is the temperature of the workpiece and T_A is the temperature of the backing bar. Khandkar et al.[1] found that using the contact gap conductance method was more accurate than the convective heat transfer coefficient. Both Simar et al.[4], Colegrove and Shercliff[5] and Shi et al.[6] have used a variable contact gap conductance in their models. Shi et al.[6] applied a temperature dependent contact gap conductance method where the value increased with temperature to simulate the better contact under the tool.

Process models can be linked to Artificial Neural Network (ANN) models to find the unknown boundary coefficients. Such models have been called ‘hybrid models’ due to the combination of the two model types. Sablani[7] and Sreekanth et al.[8] have applied similar concepts in their analysis of the heat transfer between the solid particles and a fluid. The general procedure for developing a hybrid model is[7]:

- Obtaining a group of temperature versus time curves from analytic or numerical thermal models using different boundary conditions.
- Train the ANN model using the outputs from the thermal model as inputs, while using the boundary condition inputs of the thermal model as outputs to the ANN model.
- Once the ANN has been trained, experimental thermal data is input into the trained ANN to find the corresponding boundary conditions.

ANN models have also been applied to welding processes[9]. The main purpose of this study is to investigate the thermal boundary conditions using a hybrid model of the FSW process. This will be applied to a series of welds produced with the 'Flexi-stir' FSW machine which is used to analyze the phase changes which occur during welding with synchrotron radiation. The study investigates different methods for inputting the thermal data into the ANN as well as different ANN topologies.

2 Friction stir welding experiments

The experimental FSW work was performed on 3.2 mm thick 7449-T7 plates at Helmholtz-Zentrum Geesthacht. The length of the plate was 250 mm and the width was 150 mm. The tool shoulder was flat with a scroll feature, and its radius is 6.5 mm. The threaded triflat pin had a radius at the top of 2.5 mm, and tip radius of 1.9 mm, with an overall length of 3.2 mm. The tool tilt angle was 3°. The 'Flexi-stir' machine[10] developed at Helmholtz-Zentrum Geesthacht used two backing bars: a 1 mm thick, 19 mm wide copper backing bar underneath the workpiece which was supported by two steel blocks – geometries as shown in Figure 1. A 3 mm gap was provided between the steel blocks underneath the copper backing bar. The thin copper backing bar underneath the tool allowed the synchrotron radiation to pass through the workpiece to the target while providing minimal support to the underside of the weld. The copper backing bar deformed during processing – the support provided with this setup is much poorer than that provided by a conventional backing bar. Nevertheless good thermal contact is maintained throughout: the workpiece and the copper backing deformed together during welding. In addition, the workpieces were clamped to the steel blocks and the copper bar was correspondingly clamped in-between the workpiece and the steel blocks.

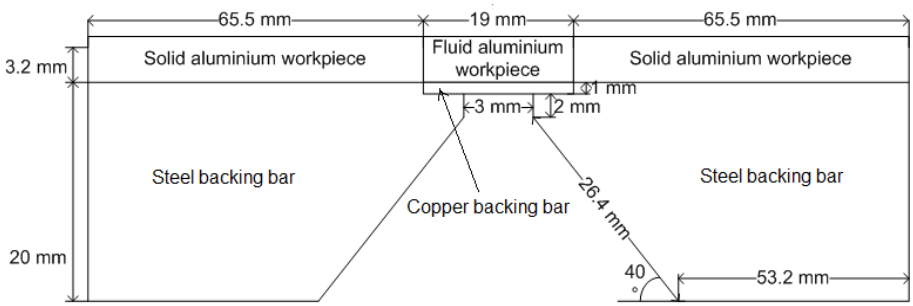

Figure 1 Diagram of the geometry used for the process model

Travel speeds of 2, 3, 4, 5, 6 and 8 mm/s with a rotation speed of 1300 rpm were used for the welds. K-type thermocouples were used for measuring the thermal profile. The thermocouples were positioned 8±0.5, 13±0.5 and 18±0.5 mm away from the centre of the weld. They were inserted into 1.6±0.1 mm deep, ø1 mm holes and a polysynthetic sliver thermal compound (including aluminium and zinc oxides particles) was applied to aid heat transfer between the thermocouple and the workpiece material. Thermal tape was used to hold the thermocouples in position. The actual position of the thermocouples was validated by measuring the distance from the centreline on the weld macrosections. The thermocouple at 8 mm away from the weld centre was within the Heat Affected Zone (HAZ) but close to the Thermo Mechanically Affected Zone (TMAZ) boundary for the 3 mm/s travel speed weld. As the travel speed increased the distance to the TMAZ boundary increased. Therefore all the thermocouples were sufficiently far from the TMAZ so their position was not affected by the welding process. This enabled direct comparison with the temperature measurements from the numerical model. The thermal profiles from the retreating and advancing sides were averaged before inputting into the ANN model. The average temperature difference between the advancing and retreating sides was measured to be 13^{o}C. The welds were completed with position control. The Flexi-stir machine did not allow measurement of either the axial load or the torque.

3 Hybrid model development

3.1 Structure of the hybrid model

The hybrid modelling procedure consists of the following steps:

1. Apply several groups of hypothetical boundary condition values to the FSW process model, and obtain the corresponding thermal data.

2. Abstract or summarise the thermal data so that the characteristics of the thermal curves can be represented by key data values.
3. Train the ANN models with the data values from step 2. Note that during training the thermal data are inputs and the boundary condition values are outputs.
4. Abstract the experimental thermal data using the same method that was used for the model data and input into the trained ANN. Obtain the predicted boundary condition values.
5. Enter the predicted boundary conditions into the FSW process model, and obtain the corresponding thermal data.
6. Compare the predicted thermal data with experimental thermal data.

3.2 FSW process model

The FSW process model is a three-dimensional fully coupled model developed with FLUENT CFD solver and is similar to that described in Colegrove and Shercliff[5]. The model was solved in the steady-state mode, which was found suitable for all travel speeds according to the procedure described in Grong[11]. This strategy resulted in a more rapid solution than a full transient simulation.

The geometry of the model is given in Figure 1. The overall geometry of the tool was described previously. The profiled features on the shoulder (scroll) and the pin (threads and flats) were ignored to simplify the mesh generation: the shoulder was modelled as an annulus and the pin as a truncated cone. In addition, the tool tilt was not included in the model. In models where the material sticks to the surface of the tool - such as the one presented in this paper – the effect of the tool features on the heat generation is minimal[12]. Ignoring the features on the tool is a common simplification in FSW process models[1, 4].

In the flow model, the Navier Stokes equation[13] is solved. The material viscosity is found from the following relationship[12]:

$$\mu = \frac{\sigma}{3\dot{\varepsilon}} \tag{1}$$

where μ is the material viscosity, σ is the material flow stress and $\dot{\varepsilon}$ is the effective strain-rate. The material flow stress was calculated from a modified version of Zener-Holloman law proposed by Sellars and Tegart[14], which is widely used for aluminium alloys[15, 16]. The Zener-Holloman equation is given by

$$Z = \dot{\varepsilon} \exp\left(\frac{Q}{RT}\right) = A(\sinh \alpha\sigma)^n \tag{2}$$

where Z is the Zener-Holloman value, T is the temperature, Q is the activation energy, R is the gas constants and α, A and n are the material constants. A modification has been made due to the specific softening happened at 720 K in 7449-T7 flow curves as mentioned by Wang[17], in which the flow stress at temperature lower than 720 K is given by

$$\sigma = \alpha^{-1} \cdot a\sinh\left[\left(\frac{Z}{A}\right)^{\frac{1}{n}}\right] - \frac{720 - T}{50 \cdot (k \cdot \ln(\dot{\varepsilon}) + m)} \tag{3}$$

where k and m are two material constant, and the values are given in Table 1. Figure 2(a) shows the modified constitutive behaviour used in this work[17], which is dependent on both temperature and strain-rate and includes softening as the temperature approaches the solidus.

Table 1: The constitutive constants for 7449-T7

Materials	Q ($Jmol^{-1}$)	A (s^{-1})	n	α (MPa)	k	m
7449-T7 aluminium	1.40E+05	5.03E+11	5.17	0.7E-02	6.99	2.14

A sticking condition was assumed between the workpiece material and the tool. Full contact between the shoulder of the tool and the workpiece material was not used. During FSW the shoulder is often not in full contact with the workpiece material, because there is often a loss of contact along the front edge due to the tilt angle. In addition, there may be some slip between the tool and the workpiece material in the real weld. One way of dealing with these issues involves applying a reduced shoulder contact radius[5]. Hence the sticking condition was only applied to the reduced shoulder contact radius and the contact shoulder radius ratio (CSRR) was defined as the ratio of the contact shoulder radius to the original radius of the tool. Since the shoulder contact radius has a direct impact on the heat generation, it is one of the adjustable parameters in the hybrid model.

Since the material movement away from the welding tool is negligible, the workpiece was divided into a liquid-like aluminium region adjacent to the tool in which the momentum and heat equations were solved, and a solid aluminium region in the far field in which only the heat equation was solved.

The heat equation was solved in the thermal model[18]. The flow stress and strain-rate from the flow model was used to calculate the viscous heat generation from the following equation[13]:

$$S_h = \nabla \cdot (\tau \cdot v) \tag{4}$$

Where S_h is the viscous heat generation, v is the velocity, τ is the stress tensor given by

$$\tau = \mu(\nabla v + \nabla v^T) \tag{5}$$

Frictional heat was not included because a sticking boundary condition was used. Both the thermal and flow models are solved iteratively until convergence is achieved.

The main difference between this model and the one reported in Colegrove and Shercliff[5] is the thermal boundary conditions due to the unique design of the machine. To model the imperfect contact between the aluminium workpiece and the backing bars, temperature dependent contact gap conductance boundary conditions were applied. According to Figure 1, there are three interfacial boundaries which need to be determined: the boundary condition between the aluminium workpiece and the copper backing bar k_1, the aluminium workpiece and the steel backing bar k_2 and between the copper and steel backing bars k_3. An experimental investigation of the contact gap conductance by Yüncü[19] showed that the values between aluminium and steel, and copper and steel were similar and approximately a quarter of the value between copper and aluminium. As stated in the introduction, temperature dependent contact gap conductance between the aluminium workpiece and steel backing bar was used by Shi et al.[6] and Rohsenow and Hartnett[20]. Although discrete values in the form of a lookup table were used, the values approximate an exponential curve. The justification for this approach can be seen in the schematic plot of contact conductance vs. temperature and pressure based on the experimental results from Zhu et al.[21] in Figure 2(b). In the far field both the temperature and interfacial pressure are low which leads to a low contact gap conductance. Near the tool, both the temperature and pressure increase leading to an exponential increase in the contact gap conductance with temperature (if the pressure is not included as a parameter). Therefore the temperature dependent contact gap conductance values in the hybrid model were represented by:

$$k_1 / 4 = k_2 = k_3 = a \cdot \exp(b \cdot T) \tag{6}$$

In which T is the temperature at the interface between the workpiece and backing bar in Kelvin, and a and b are constants to be determined with the hybrid model.

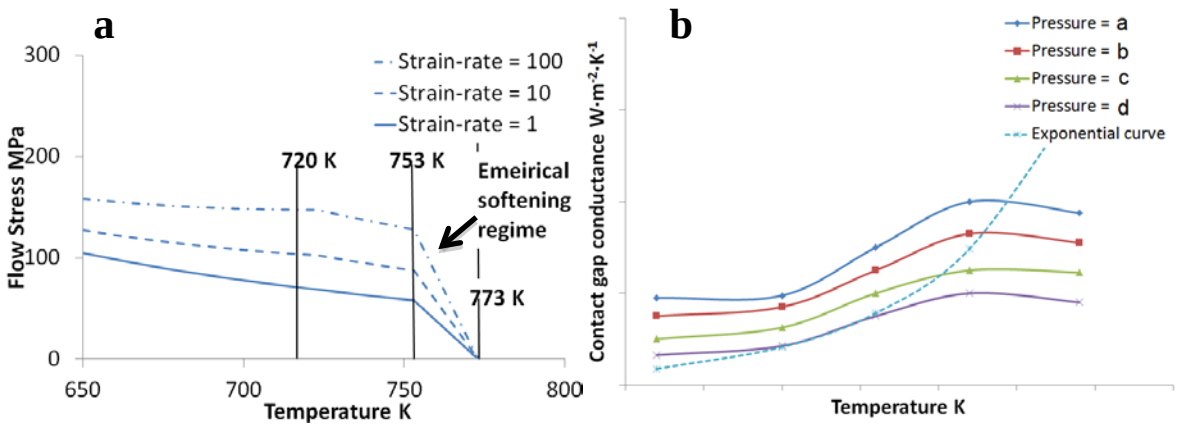

Figure 2 (a) Material flow stress as a function of temperature and strain-rate for 7449-T7 aluminium alloy[17], and (b) schematic plot of contact gap conductance vs. temperature and pressure based on values from Zhu et al.[21], note the pressure values from large to small is a, b, c and d, and numerical values for axis are not included due to copyright consideration.

The convective heat loss from the top surface of aluminium workpiece was 10 W/m^{2}K (Chao and Qi[22]) and the convective heat loss from the bottom of the steel backing bars was 1000 W/m^{2}K which was used by Colegrove and Shercliff[5]. The thermal material properties of the materials used in the model are shown in Table 2.

Table 2 Thermal properties of the materials used in the FSW process model.

Material name	Density (kg·m^{-3})	Specific heat (J·Kg^{-1}·K^{-1})	Thermal conductivity (W·m^{-1}·K^{-1})
7449-T7 aluminium workpiece[23]	2840	860	154
Copper backing bar[24]	8954	383	386
Backing bar steel (0.5% C steel) at 150°C[24]	7833	465	40
H13 tool steel (5% chrome) at 300°C[24]	7833	460	36

Describing the material flow behaviour is one of the most essential parts for modelling the FSW process. This work used a modified version of Zener-Holloman law proposed by Sellars and Tegart[14], which is widely used for aluminium alloys[15, 16]. Figure 2 shows the modified constitutive behaviour used in this work, which includes softening as the temperature approaches the solidus.

3.3 Artificial neural network model development

As described in section 3.1, the aim of the ANN is to find the values of the CSRR, and contact gap conductance parameters, *a* and *b*. Travel speed was not included because it was

known from the welding experiment. One of the key requirements of the hybrid model was abstracting the thermal curves before inputting them into the ANN. Several abstracting methods were investigated and are shown in Figure 3 and are summarised in Table 2.

The three methods are the peak temperature, cooling slope and integral of temperature. The cooling slope is the slope of the line between the peak temperature and the temperature at half this value. When calculating the integral, the time over which the temperature was integrated varied for the different travel speeds, and equalled the length of plate divided by the travel speed. The three methods were applied at distances of 8, 13 and 18 mm from the weld centreline, which correspond to the location of the thermocouples.

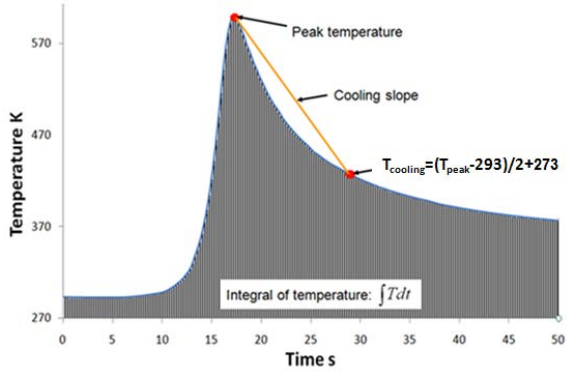

Figure 3 Methods for abstracting the thermal profile.

Table 3 Summary of abstracting methods used for the hybrid ANN models.

Abstracting Method	**Parameters**	**Thermocouple positions – distance (mm) from weld centerline.**
9 input	Peak temperature, integral of temperature, and cooling slope	8, 13 and 18
6 input-p-i	Peak temperature, and integral of temperature	8, 13 and 18
6 input-p-c	Peak temperature, and cooling slope	8, 13 and 18
6 input-i-c	Integral of temperature, and cooling slope	8, 13 and 18
4 input-p-i	Peak temperature, and integral of temperature	8 and 18
4 input-p-c	Peak temperature, and cooling slope	8 and 18
4 input-i-c	Integral of temperature, and cooling slope	8 and 18

The fundamental components of the ANN model are the ANN topology, transfer function and training algorithms[25]. The overall applied transfer function was the sigmoid equation. The back propagation algorithm was used throughout the study with the Levenberg-Marquardt (LM) gradient decent method. Three ANN topologies were investigated in this study:

1. The multilayer perceptrons network (MLP) with three hidden layers: 9 in the first, 6 in the second and 3 in the third.
2. The generalized feedforward network (GFF) with three hidden layers: 9 in the first, 6 in the second, and 3 in the third.
3. The modular feedforward network (MFF) with three hidden layers: 5 in the first, 5 in the second and 5 in the third.

To train the hybrid model, three CSRR values and four values of the backing bar constants *a* and *b* were used, giving forty-eight combinations at each travel speed. The applied values are shown in Table 4.

Table 4: The training data used for the hybrid model

CSRR	*a* (W $m^{-2}K^{-1}$)	*b* (K^{-1})
43.2%	8	0.005
55.4%	21	0.01
75.7%	38	0.012
	43	0.015

To compare the predicted thermal profiles with the experimental curves the mean relative error (MRE) was found using:

$$MRE = \left(\sum_{i=1}^{N} \left| \left(Y_i - X_i \right) / X_i \right| \right) \Big/ N \qquad (7)$$

where X_i and Y_i are the abstracted peak temperature, integral of temperature vs. time and cooling slope from the model and experiments respectively.

4 Results and discussion

4.1 Topology and abstraction method investigation

The average prediction qualities were calculated by averaging across the six travel speeds for each abstracting method and ANN topology and are shown in Figure 4 with the error bars indicating the 95% confidence interval of the mean. Overall, the difference in MRE values for the different abstracting methods is relatively small, particularly when taking into account the variance in the mean which is also shown in Figure 4. Nevertheless, the 4 input-i-c method which used the integral of temperature vs. time and the cooling slope had consistently lower MRE for the three ANN topologies. The lowest overall MRE was obtained when the GFF topology was used with this abstracting method. Table 5 shows the individual MRE values at the different travel speeds for this abstracting method and indicates that the MRE was greatest for the 4 mm/s travel speed.

Hence the additional information provided by the 6 and 9 input methods which include the peak temperature at more locations did not lead to any improvement in the overall prediction quality. Any changes in the overall temperature were captured adequately by the integral of temperature against time with the 4 input-i-c method. Of the 3 ANN topologies, the GFF method provided the best predictions.

Table 5 MRE for the 4 input-i-c abstracting method with GFF topology for the different travel speeds.

2 mm/s	3 mm/s	4 mm/s	5 mm/s	6 mm/s	8 mm/s	Average
3.34%	1.93%	5.61%	3.18%	2.35%	2.01%	3.07%

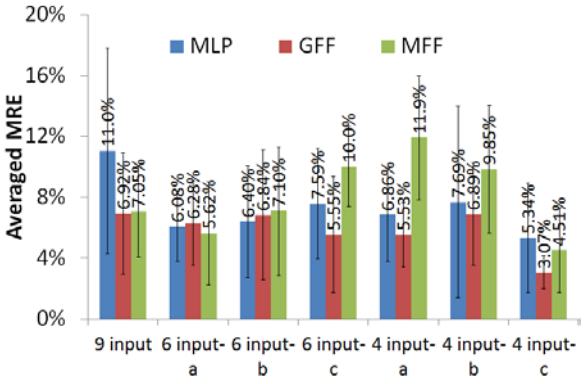

Figure 4: Average MRE for the different abstracting methods and ANN topologies including the 95% confidence interval of the mean. Note that the different abstracting methods are defined in Table 3.

A visual comparison between the experimental measurements and those from the 4 input-i-c method are shown in Figure 5. The comparison shows that all the predicted curves were able to give good predictions of the thermal cycles, particularly the peak temperature. In most cases the hybrid models were able to give accurate predictions of the cooling slopes.

The predicted CSRR and boundary conditions for the different travel speeds are shown in Table 6 for this abstracting method and topology. The predicted values of the contact gap conductance parameters, *a* and *b* from Table 6 were used to plot the contact gap conductance as a function of temperature in Figure 6. The visual comparisons and the predicted values in Table 6 suggest that the thermal boundary condition performance and the CSRR are not independent of each other. For instance, the 5 mm/s case had a larger contact gap conductance, while the CSRR value is also higher at 70.9%. Hence the larger CSRR, which resulted in more heat being generated, is balanced by a higher contact gap conductance which increased the heat loss. The situation is also complicated by variations in the welding process. These issues are investigated in greater depth in the next section.

Table 6: Predicted values of CSRR, and contact gap conductance coefficients *a* and *b* from the 4 input method-i-c hybrid model.

Travel Speed	CSRR	a ($W\ m^{-2}K^{-1}$)	b (K^{-1})
2 mm/s	63.9%	43.5	4.56E-03
3 mm/s	43.2%	44.9	4.54E-03
4 mm/s	74.7%	44.6	4.46E-03
5 mm/s	70.9%	6.32	1.04E-02
6 mm/s	75.7%	6.06	4.91E-03
8 mm/s	51.9%	6.56	5.20E-03
Average values	63.4%	25.3	5.67E-03

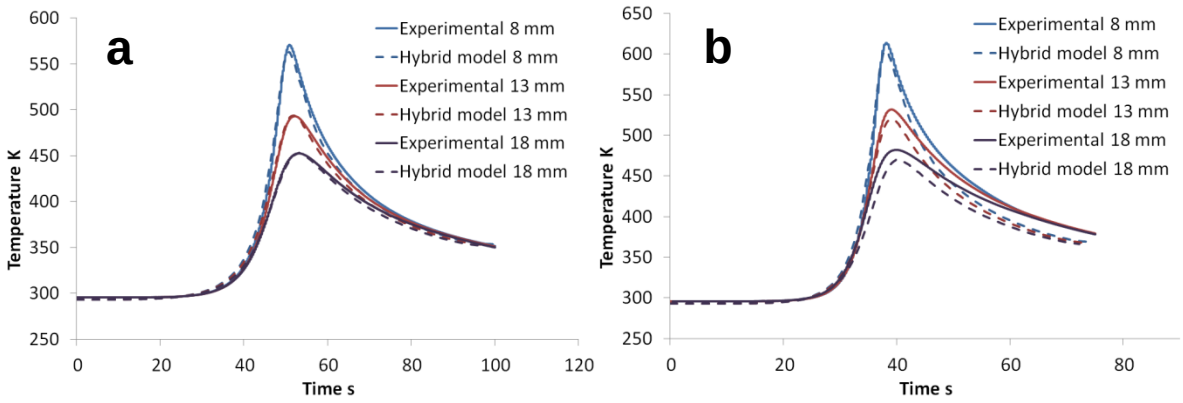

Figure 5: Comparison between the thermal profiles predicted from the hybrid model that used the 4 input-i-c abstracting method with GFF topology, and the experimental thermal profiles for travel speeds of the best fitting one a) 3 mm/s and the worst b) 4 mm/s

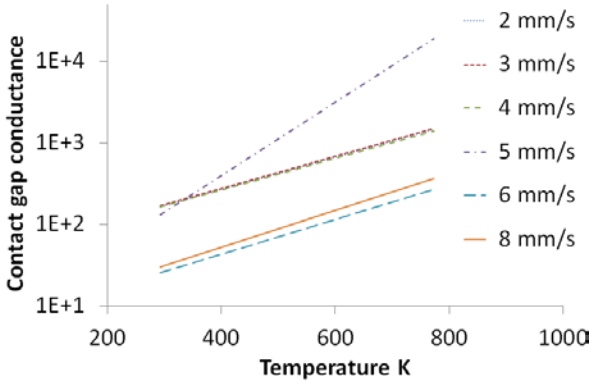

Figure 6: Contact gap conductance vs. temperature from the predicted contact gap conductance coefficients, *a* and *b* in Table 6.

4.2 Investigation into variable fitting constants

Colegrove and Shercliff[5] showed that it was possible to find a universal set of fitting constants that suit all welding parameters. The previous section found that the fitting constants depended on the travel speed. Therefore the average values from Table 5 were applied to each of the welds, and the quality of the fit was determined.

The cooling slope was predicted well in all cases. However there were some discrepancies in the peak temperature which are summarised in Figure 7. The predictions for the 2, 5 and 8 mm/s welds were reasonably good with the difference in the peak temperature being less than 16 K. The 4 and 6 mm/s models have largely under-predicted the experimental results, while the 3 mm/s model largely over-predicted the experimental results.

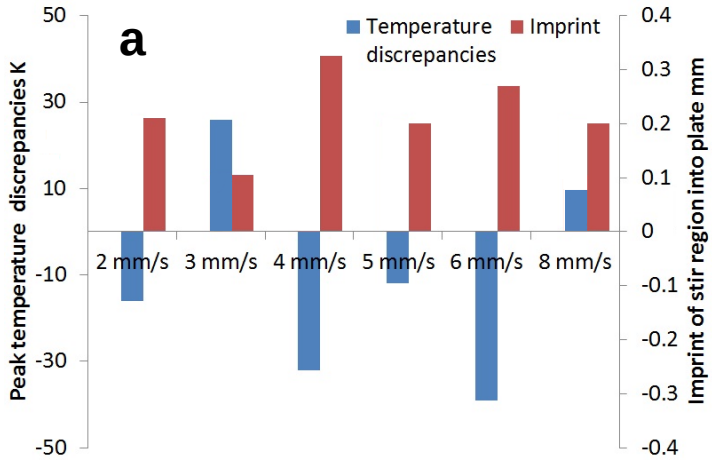

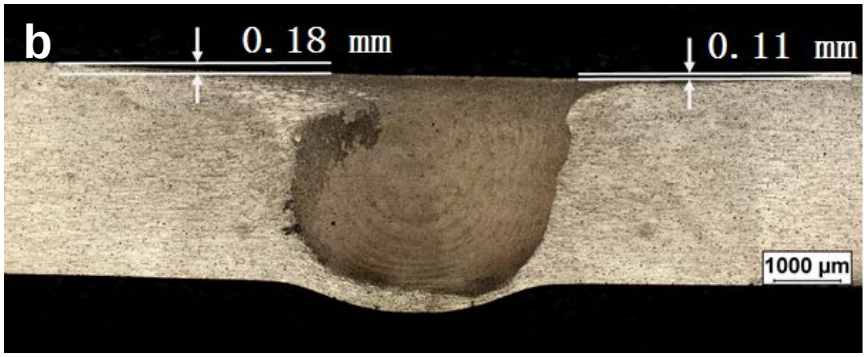

Figure 7: (a) Discrepancies in the peak temperature (positive for over-prediction and negative for under-prediction) between the experimental and predicted thermal curves with averaged fitting coefficients; and measured imprint of the stir region into the plate; (b) Measurement of the imprint of the FSW tool into the workpiece material. This particular macro is from the 3 mm/s travel speed weld where there was less penetration.

One of the reasons for variability in thermal measurements between nominally identical welding conditions is the plunge depth or the plunge force (depending on whether the FSW machine works in force or displacement control). Tang et al.[26] showed that the temperature increases with plunge depth. The Flexi-stir machine used displacement control and different values were used for the different welding conditions. To understand the variation in displacement between the welds, the imprint of each weld into the plate was measured as shown in Figure 8. Note that considerable deformation occurred under the weld due to the copper backing bar used for Flexi-stir machine (see Figure 1). The imprints were measured on both sides of the weld stir region, and the values averaged. These values are summarised in Figure 7(a).

The results showed that where there was a good temperature prediction, (2, 5 and 8 mm/s) the imprint depth was approximately 0.20 ± 0.01 mm. For the 3 mm/s weld, the temperature was over-predicted by the model and the imprint was only 0.105 mm. This indicates that during the welding process, the tool position was higher compared to those with an imprint of 0.2 mm. Hence the contact between the shoulder and the material was poorer, leading to less heat generation. This was also reflected in a lack of coalescence defect for this weld which is shown in Figure 7(b). The poorer prediction may also from due to a poor contact between the workpiece and the copper backing bar from the plate lifting reflected by the large bulge on the bottom of the workpiece. For the 4 and 6 mm/s welds, the temperature values were under-predicted by the model. The imprint depths were 0.325 and 0.27 mm, for these welds indicating that the tool plunged further into the material. This leads to better contact with the material and greater heat generation, so the model under-predicted the temperature. Therefore the discrepancies between the model that used averaged input parameters and the experiments may be due to the variability in the plunge depth used during the welding experiments.

5 Conclusions

A hybrid model of FSW was developed by combining a process model with an ANN model. The technique was used to investigate the thermal boundary conditions at the interface between the workpiece and backing bar, as well as the CSRR. It was demonstrated that:

- The hybrid model was able to predict suitable values for the temperature dependent thermal boundary condition parameters and the CSRR.
- A GFF topology for the ANN with 4 abstracted inputs based on the integrated temperature vs. time and the cooling slope gave the best prediction of the experimental temperature.
- The analysis indicated that the CSRR and the thermal boundary conditions were not independent of each other. Hence a high CSRR could be offset by a high heat loss to the backing bar.
- Although the initial analysis indicated that it was not possible to find a universal set of fitting parameters for these welds, further analysis indicated that when average values were applied across the welds good predictions of the weld thermal cycles were obtained across the travel speeds. The variability which was observed could be attributed to the variation in the plunge depth which was reflected in the weld imprints.

6 Acknowledgements

The authors would like to acknowledge the support from the Virtual Institute for Improving Performance and Productivity of Integral Structures through Fundamental Understanding of Metallurgical Reactions in Metallic Joints (VI-IPSUS). The VI-IPSUS is an initiative of the Helmholtz Association coordinated by the Helmholtz-Zentrum Geesthacht.

References

1. M. Z. H. Khandkar, J. A. Khan, and A. P. Reynolds: 'Prediction of temperature distribution and thermal history during friction stir welding: Input torque based model', *Science and Technology of Welding and Joining*, 2003, 8(3), 165-174.
2. R. Nandan, G. G. Roy, T. J. Lienert, and T. Debroy: 'Numerical modelling of 3D plastic flow and heat transfer during friction stir welding of stainless steel', *Science and Technology of Welding and Joining*, 2006, 11(5), 526-537.
3. A. Arora, R. Nandan, A. P. Reynolds, and T. DebRoy: 'Torque, power requirement and stir zone geometry in friction stir welding through modeling and experiments', *Scripta Materialia*, 2009, 60(1), 13-16.
4. A. Simar, T. Pardoen, and B. De Meester: 'Effect of rotational material flow on temperature distribution in friction stir welds', *Science and Technology of Welding and Joining*, 2007, 12(4), 324-333.
5. P. A. Colegrove, H. R. Shercliff, and R. Zettler: 'Model for predicting heat generation and temperature in friction stir welding from the material properties', *Science and Technology of Welding and Joining*, 2007, 12(4), 284-297.
6. Q. Shi, T. Dickerson, and H. R. Shercliff: 'Thermomechanical FE modeling of friction stir welding of Al-2024 including tool loads', *Proceedings of 4th International Friction Stir Welding Symposium*, 2003, Park City, UT, USA.
7. S. S. Sablani: 'A neural network approach for non-iterative calculation of heat transfer coefficient in fluid-particle systems', *Chemical Engineering and Processing: Process Intensification*, 2001, 40(4), 363-369.
8. S. Sreekanth, H. S. Ramaswamy, S. S. Sablani, and S. O. Prasher: 'A neural network approach for inverse heat transfer problems', *American Society of Mechanical Engineers National Heat Transfer Conference*, 1997, Baltimore, MD, USA.
9. D. Weiss, K. H. Christensen, and J. K. Kristensen: 'Computerised calibration of thermal welding models', in 'Mathematical modelling of weld phenomena 8', (eds. H. Cerjak, et al.), 469-484; 2007, TU Graz.
10. Z. R. B. M. R. A. L. H. d. S. J. F. Sheikhi S: Patent Applications (‘FlexStir’): 102005029882.6 (DE), and 102005029881.8 (DE), 2005.
11. Ø. Grong: 'Metallurgical modelling of welding', *Book.Second Edition.Publ: London SW1Y 5DB, UK; Institute of Materials; 1997.ISBN 1-86125-036-3*.
12. P. A. Colegrove and H. R. Shercliff: '3-dimensional CFD [computational fluid dynamics] modelling of flow round a threaded friction stir welding tool profile', *Journal of Materials Processing Technology*, 2005, 169(2), 320-327.
13. FLUENT User's Manual, FLUENT Inc., (12^{ed}. Release), 2006, Lebanon, NH, USA.
14. C. M. Sellars and W. J. M. Tegart: 'Hot workability', *Int. Met. Rev.*, 1972, 17, 1-24.
15. R. Carmona, Q. Zhu, C. M. Sellars, and J. H. Beynon: 'Controlling mechanisms of deformation of AA5052 aluminium alloy at small strains under hot working conditions', *Materials Science and Engineering A*, 2005, 393(1-2), 157-163.

16. V. M. Sample, G. L. Fitzsimons, and A. J. DeArdo: 'Dynamic softening of copper during deformation at high temperatures and strain rates', *Acta Metallurgica*, 1987, 35(2), 367-379.
17. H. Wang: 'Numerical and artificial neural network modelling of friction stir welding', PhD thesis, Cranfield University, 2011.
18. H. S. Carslaw and J. C. Jaeger: 'Conduction of heat in solids', *Oxford University Press.*, 1959.
19. H. Yüncü: 'Thermal contact conductance of nominaly flat surfaces', *Heat and Mass Transfer/Waerme- und Stoffuebertragung*, 2006, 43(1), 1-5.
20. W. M. Rohsenow and J. P. Hartnett, *Handbook of Heat Tranfer*, 1973.
21. D. Zhu, L. Zhang, J. Pei, G. Zhang, and R. Wei: 'Experiment research on the thermal contact conductance during solid plastic forming', *Suxing Gongcheng Xuebao/Journal of Plasticity Engineering*, 2008, 15, 284-197.
22. Y. J. Chao and X. Qi: 'Thermal and thermo-mechanical modeling of friction stir welding of aluminum alloy 6061-T6', *Journal of Materials Processing and Manufacturing Science*, 1998, 7(2), 215-233.
23. P. A. Colegrove and H. R. Shercliff: 'CFD modelling of friction stir welding of thick plate 7449 aluminium alloy', *Science and Technology of Welding and Joining*, 2006, 11(4), 429-441.
24. J. P. Holman: 'Heat transfer'; 1986, New York, McGraw-Hill Book Co.
25. M. H. Hassoum: 'Fundamentals of artificial neural networks', *Mit Press, Cambridge.*, 1995.
26. W. Tang, X. Guo, J. C. McClure, L. E. Murr, and A. Nunes: 'Heat input and temperature distribution in friction stir welding', *Journal of Materials Processing and Manufacturing Science*, 1998, 7(2), 163-172.